Hindawi
Geofluids
Volume 2020, Article ID 8812564, 16 pages
https://doi.org/10.1155/2020/8812564

Research Article

A Comparison of Simplified Modelling Approaches for Performance Assessment of Piles Subjected to Lateral Spreading of Liquefied Ground

Yung-Yen Ko[1] **and Yu-Ying Lin**[2]

[1]*Department of Civil Engineering, National Cheng Kung University, Tainan 70101, Taiwan*
[2]*National Center for Research on Earthquake Engineering, National Applied Research Laboratories, Taipei 10668, Taiwan*

Correspondence should be addressed to Yung-Yen Ko; yyko@mail.ncku.edu.tw

Received 4 June 2020; Revised 9 September 2020; Accepted 11 September 2020; Published 5 October 2020

Academic Editor: Ryosuke Uzuoka

The lateral spreading of the ground due to liquefaction during earthquakes may considerably damage the embedded piles, which is an important issue in the seismic design of pile foundations. In this paper, nonlinear pseudostatic analyses were performed for the responses of piles subjected to actions of laterally spreading ground, which were modelled as flow displacement and flow pressure, respectively. The former is a displacement-based approach, in which the free-field ground displacement profile is assigned to the pile-soil interaction system; while the latter is a force-based approach, which regards the actions of laterally spreading ground as flow pressure and directly applies it to the pile. The concept of the Winkler foundation was utilized to account for the interaction between pile and soil. The soil springs with elastic-plastic *p-y* curves were used to describe the relationship of soil reaction versus lateral displacement around the pile. The distributed plastic hinges were deployed to simulate the possible flexural failure of the pile. One of the pile failure cases caused by liquefaction-induced lateral spreading in the 1995 Kobe Earthquake was adopted for case study. The analyzed pile response to flow displacement and flow pressure was compared with the field observations, and the validity and capability of both approaches were accordingly discussed. The influence of axial load on laterally loaded piles, namely, the P-delta effect was also examined. These results help to reasonably assess the performance of piles subjected to lateral spreading of liquefied ground.

1. Introduction

Pile foundations are common for their excellent bearing capacity and displacement control capability. The lateral resistance is one of the most important functions of piles in seismic active areas such as Japan and Taiwan, because it helps to withstand earthquake loading. However, the lateral resistance of a pile is mainly attributed to shallow soil layers because its deflection when laterally loaded is larger near the ground surface, where generally higher liquefaction potential is exhibited than at a greater depth for liquefiable ground due to lower overburden stress. Therefore, the seismic performance of piles may be significantly influenced by soil liquefaction.

During earthquakes, not only the lateral inertia loads transmitted from the superstructure but also the actions of lateral spreading of liquefied ground could be applied to piles, and the latter are usually more destructive because the lateral resistance of the pile is simultaneously reduced because the stiffness and strength of soil are degraded by liquefaction. Concerning piles embedded in laterally spreading ground, usually, the flexural failure is dominant because of the considerable bending moment generated by the actions of lateral spreading. Buckling instability may also occur for slender piles due to the combination of axial load and lateral deflection, namely, the P-delta effect [1], as well as the loss of lateral confinement because of the degradation of liquefied soil. Many cases have been reported, mostly related to

foundations of structures near waterfront, such as bridges along or across rivers, or wharves, tanks, and buildings in the port area.

Therefore, this study aims to investigate the lateral performance of piles subject to the actions of lateral spreading of the ground triggered by liquefaction. The widely used the Winkler foundation model, in which the pile is simulated by beam-column elements (also known as frame elements) and soil reactions are simulated by spring elements along the pile, is utilized to represent the pile-soil interaction. Elastic-plastic relationships between soil reaction (p) and lateral displacement (y), namely, p-y curves, are used to define the soil springs. The distributed plastic hinge method is adopted to simulate the possible flexural failure of the pile. Thus, the nonlinear behavior of the pile-soil system can be well exhibited at a reasonable analysis cost. In engineering practice, the actions on piles due to the lateral spreading of the liquified ground are usually simplified as flow displacement, which is also known as the displacement-based approach, e.g., [2, 3], or as flow pressure, which is also known as the force-based approach, e.g., [2, 4], and both will be introduced herein. In addition, a case study of pile failure caused by laterally spreading ground in the 1995 Kobe Earthquake using both modelling approaches will be presented and compared, and their validity and capability will be discussed. The investigation of the influence of axial load on pile performance against lateral spreading will also be included. Results of this study can be therefore served as the reference of the seismic performance assessment of piles embedded in liquefiable ground.

2. Pile Damage due to Lateral Spreading of Liquefied Ground

2.1. Liquefaction-Induced Lateral Spreading. During earthquakes, finite lateral displacement of gently sloping ground underlain by liquefied soil such as loose sands with a shallow groundwater table may occur due to the build-up of excess pore pressure or even liquefaction in the underlying deposit, as shown in Figure 1(a) [5]. This is often called the lateral spreading of the ground. Gently sloping means a slope less than 6%, or the flow failure may occur [6]. A steep free face giving an unrestricted boundary, e.g., riverbank or seashore, is common in lateral spreading.

The profile of laterally spreading ground is shown in Figure 1(b), which can be divided into a nonliquefied (unsaturated, impervious, or clayey) surface layer (so-called crust layer) and a liquefied (saturated, loose, and sandy) underlying layer. Tension cracks or ground fissures perpendicular to the direction of spreading as well as slumping are often found on the ground surface, especially near the upper margins of the spreading area.

2.2. Actions of Lateral Spreading on Piles. Based on the observations in the 1995 Kobe Earthquake, the pile foundations embedded in liquefied and laterally spreading ground were damaged mainly due to the kinematic forces arising from horizontal ground displacement, and for friction piles, settlement and tilting with the adjacent ground surface were caused [7]. The pile response in liquefiable soils can be differentiated as cyclic phase and lateral spreading phase [8]. In the former, inertial forces mainly from the superstructure are dominant, while in the latter, they play an important role only at the onset of lateral spreading because the shaking intensity diminishes as the spreading progresses. On the other hand, the kinematic load induced by the lateral ground movement becomes the controlling factor of the pile response in the lateral spreading phase.

The actions of lateral spreading on piles can be further examined experimentally via the induced lateral pressure, or, soil reaction to the piles. Brandenberg et al. [9] found through centrifuge tests that the nonliquefied crust displaced more than the liquefiable layer and imposed larger soil reaction on the pile, yet large relative displacements between the pile and the crust were required to mobilize peak crust loads acting on the pile. In contrast, actions from the liquefiable layer could be complex if the crust pulled the pile downslope such that the downslope movement of the pile was greater than that of the liquefiable soil, which was possible for more flexible piles. Haeri et al. [10] reported based on 1-g shaking table tests that the maximum lateral soil pressure along the piles in liquefiable layer increased almost linearly with the depth, namely, showed approximately a triangular pattern same as the simplified flow pressure profile due to lateral spreading proposed by Japan Road Association (JRA) [4], which will be introduced later; however, the observed maximum pressures were higher than those specified in [4] for a single pile, yet were reasonably in agreement for piles with neighboring ones. According to the observations in a large scale 1-g shaking table test, Motamed et al. [11] concluded that the JRA simplified flow pressure seemed appropriate for closely spaced pile groups, which is conformable to [10], and was therefore considered useful in preliminary analysis.

2.3. Cases of Pile Damage Related to Lateral Spreading. In the 1964 Niigata Earthquake, soil liquefaction and its devastating effects started to catch the attention of engineers. For example, a public building suffered flexural failure of piles which concentrated at the interface of the liquefied and nonliquefied layers because the lateral spreading induced permanent ground displacement, and piles moved by nonliquefied soil layers were even worse damaged [12]. Another widely known case is the collapse of the Showa Bridge possibly, which was possibly due to the combined effect of axial load and lateral spreading which led to buckling instability of piles [1].

The Mw 6.9 1995 Kobe Earthquake brought severe damages to reclaimed lands along the shoreline of Kobe City, especially in the Port of Kobe, mainly because of liquefaction and lateral spreading [13]. Several facilities and buildings experienced pile failure caused by laterally spreading ground. In a pile-supported wharf, a horizontal displacement up to 1.7 m at the deck and local buckling of the steel pipe piles associated with significant lateral deformation of the sand layer were observed [14]. The seaward movement of a quay wall damaged the precast concrete (PC) piles of a nearby oil-storage tank in terms of lateral deformation and flexural cracks, which were

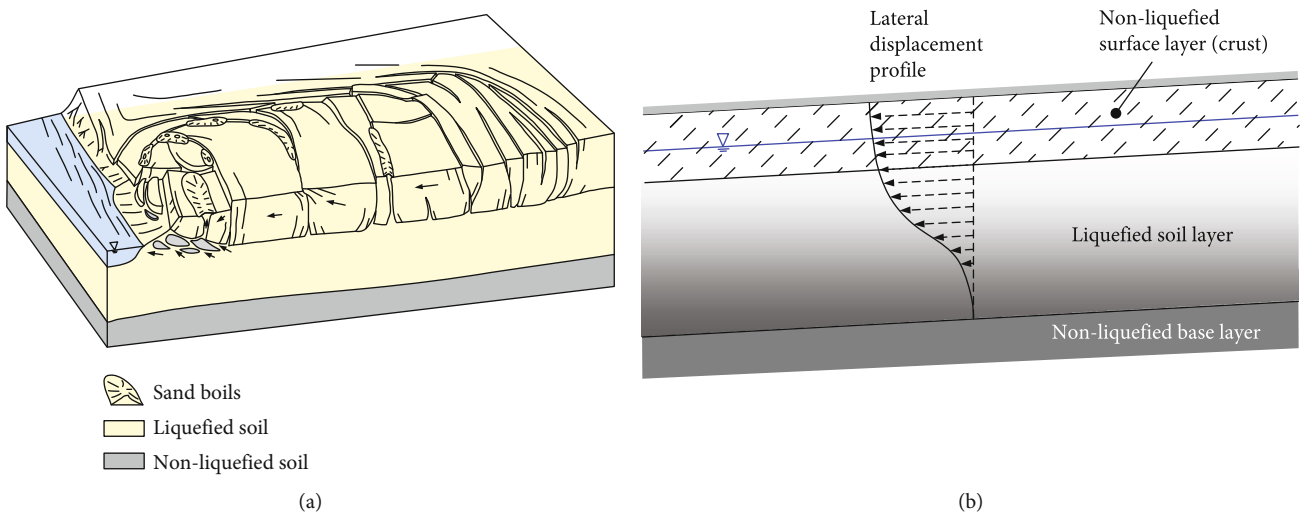

Figure 1: Liquefaction-induced lateral spreading. (a) Schematic depiction. (b) Lateral displacement profile. (After [5]).

more severe near the interface of the liquefied fill deposit and underlying silty soil layer [15]. The PC piles of a building near the waterfront were severely cracked and even broken due to a displacement above 1.5 m of the quay wall, which led to considerable tilting of the superstructure [16], which was adopted for case study in this paper and more details will be given later.

A more recent case was reported in the 2016 Kaikoura, New Zealand Earthquake, that a lateral spreading with a displacement of 0.8-1.0 m at the edge of the fill pushed a pile-supported wharf to a tilt of 1~2.5° and a seaward moment of 0.2~0.5 m [17].

3. Modelling of Actions of Lateral Spreading on Piles

Figure 2(a) shows the typical condition of a pile undergoing lateral spreading of liquefied ground. The moving soil body leans against the pile; meanwhile, the soil reaction to provide lateral resistance of the pile is reduced due to liquefaction. Flexural deformation and bending moment of the pile are thus caused. Lateral spreading is even damaging if there is a nonliquefied surface layer, which is also known as the crust layer because its interaction with the pile is more significant. Two methods which are common in engineering practice for the modelling of these actions are introduced as follows.

3.1. Lateral Spreading as Flow Displacement. Firstly, the free-field ground displacements profile due to lateral spreading is estimated and then assigned as the boundary conditions to the free ends of the soil springs (other than those ends attached to the pile) in the liquefied layer, as shown in Figure 2(b). It might be necessary to reduce the subgrade reaction coefficients or the *p-y* curves of the soil springs based on the liquefaction potential of the corresponding soil layers to account for the degradation of liquefied soil. Then, forced displacement analysis can be accordingly performed.

The simplified approximation of liquefaction-induced ground displacement proposed by Tokimatsu and Asaka [18] was adopted in this study. The horizontal displacement of the ground surface, $D(x)$, at a distance from the waterfront of x can be approximated as:

$$D(x) = D_0 \left(\frac{1}{2}\right)^{5x/L_{ls}} \tag{1}$$

where $D_0 = D(x = 0)$, denoting the horizontal displacement of the ground surface at the waterfront, and L_{ls} is the length of the laterally spreading area. Based on the field data of ground displacement induced by lateral spreading in the1995 Kobe Earthquake, $L_{ls} = (25 \sim 100)\, D_0$, and $L_{ls} = 50\, D_0$ can be regarded as representative.

Then, the ground displacement profile of a laterally spreading deposit, $d_{ls}(z, x)$, at a distance from the waterfront of x can be approximated as:

$$\begin{aligned} d_{ls}(z,x) &= D_0 \left(\frac{1}{2}\right)^{x/(10\,D_0)} && \text{for } 0 \le z < z_w \\ d_{ls}(z,x) &= D_0 \left(\frac{1}{2}\right)^{x/(10\,D_0)} \cos\left[\frac{\pi(z - z_w)}{2H_L}\right] && \text{for } z \ge z_w \end{aligned}, \tag{2}$$

where z is the depth below the ground surface; z_w and H_L denote the depth at the top of the liquefied layer and its thickness, respectively.

3.2. Lateral Spreading as Flow Pressure. As shown in Figure 2(c), the actions of lateral spreading are represented by flow pressure directly imposed on the pile. JRA [4] proposed that the flow pressure profile in the nonliquefied crust layer with respect to the depth z, $q_{NL}(z)$, and that in the liquefied layer, $q_L(z)$, can be expressed as:

$$q_{NL}(z) = c_s c_{NL} K_P \gamma_{NL} z \quad \text{for} \quad 0 \le z \le H_{NL}, \tag{3}$$

$$q_L(z) = c_s c_L [\gamma_{NL} H_{NL} + \gamma_L (z - H_{NL})] \text{for} \quad H_{NL} < z \le H_{NL} + H_L, \tag{4}$$

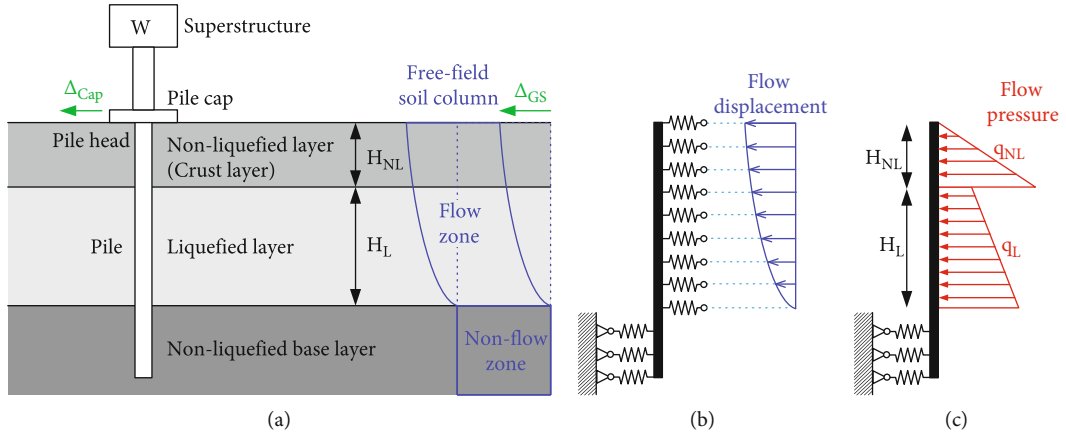

Figure 2: Actions of lateral spreading on pile. (a) Typical condition. (b) Modelled as flow displacement. (c) Modelled as flow pressure.

where K_P is the passive earth pressure coefficient; H_{NL} and H_L are the thickness, and γ_{NL} and γ_L are the unit weight of the nonliquefied crust and liquefied layers, respectively; c_L is the modification factor for flow pressure in the liquefied layer, which is suggested to be 0.3, while that in the nonliquefied layer, c_{NL}, is based on the liquefaction potential index (often denoted as P_L or LPI) defined in [19]; c_s is the modification factor based on the distance from the waterfront. Suggested values of c_{NL} and c_s are listed in Table 1.

As mentioned in Section 2.2, this simplified pressure profile in liquefied layer can be considered reasonable for closely spaced piles [10, 11], and to mobilize the flow pressure in the nonliquefied layer, which is regarded as passive earth pressure in [4], large relative displacements between piles and soil are needed [9]. In addition, it is noted that the flow zone in Figure 2(a) induces flow pressure but provides no soil reaction, while the nonflow zone induces no flow pressure but provides soil reaction.

4. Case Study

4.1. Case Introduction. A 3-story building located at the coastal area of Kobe City which suffered pile damage due to lateral spreading of liquefied ground during the 1995 Kobe Earthquake [16], as mentioned in Section 2.3 and as shown in Figure 3, was adopted for case study. This lateral spreading induced a seaward movement of about 1.6 m of a neighboring quay wall at the waterfront, and a ground surface displacement around 0.9~1.1 m was observed at the base of the building. 38 PC piles which had a length of 20 m and a hollow cross-section with an outer diameter of 400 mm and a wall thickness of 65 mm were installed for this building by preboring method. Pile S-7 and Pile N-7 in Figures 3(a) and 3(b) suffered horizontal and longitudinal cracks at the pile head and near the interface between the reclaimed fill and the underlying sand layer (at a depth of about 9 m), and Pile S-7 was even broken at a depth of 4.5 m with a crack up to 40-100 mm wide. The superstructure was therefore tilted about 3° (or, 1/18).

The boring data of the site from [16] are shown in Figure 3(c), and the corresponding soil types and blow counts of standard penetration test (SPT-N) are listed in Table 2. The SPT-N values of the reclaimed fill were mostly no more than 10, and this layer could be in a loose state. The sand layer had SPT-N ranged from 14 to 24 and was probably medium dense. Low SPT-N values were noticed in the sandy silt layer, and a relatively high fine content (FC) could be expected though the data were not available. The gravelly sand layer was stiff for its high SPT-N up to 50. Considering a horizontal peak ground acceleration (PGA) of 300 gal based the real earthquake record at a reclaimed land as well as a groundwater level at a depth of 2 m [16], the liquefaction potential was assessed using the simplified procedure proposed by Architectural Institute of Japan (AIJ) [20], which was considered more reasonable in general because it included the influence of fine content on liquefaction potential, as well as the cyclic mobility of dense sand in the reduction of stiffness and strength of liquefied soil [21]. In calculating the factor of safety against liquefaction (F_L) of a soil layer, its cyclic resistance ratio (CRR) is determined by the SPT-N corrected based on the FC values, which were assumed based on the soil types given in [16]. The soil layer is considered liquefied if $F_L < 1$, yet the sandy silt layer was directly regarded as nonliquefiable (N.L.) herein because of its high fine content. The results are given in Table 2, indicating that the upmost nonliquefied (crust) layer above the groundwater table with a thickness around 1~2 m was underlain by a liquefied layer with a thickness around 7~8 m, which was basically the reclaimed fill, and beneath the liquefied layer was the lower nonliquefied layer comprised of sand, sandy silt, and gravelly sand. These results are conformable to [16]. In addition, the reduction factors (D_E) for the mechanical parameters of liquefied soil suggested in [20] based on F_L and SPT-N are also included in Table 2, and D_E will be used in the following analysis to reduce the *p-y* curves for the liquefied layer.

It is noted that the cracks of the piles at a depth of 9 m were in fact at the interface between the liquefied and lower nonliquefied layers, and the breakage at a depth of 4.5 m was within the liquefied layer, close to where $D_E = 0$.

4.2. Analysis Model. The structural analysis software SAP2000 was adopted to perform nonlinear pseudostatic analysis for the response of piles subjected to lateral

Table 1: Modification factors for flow pressure [4].

P_L	c_{NL}
$P_L \le 5$	0
$5 < P_L \le 20$	$(0.2P_L - 1)/3$
$P_L > 20$	1
Distance to waterfront, s (m)	c_s
$s \le 50$	1.0
$50 < s \le 100$	0.5
$s > 100$	0

spreading. The P-delta effect, which involves large tensile or compressive stresses on transverse bending and shear behavior, and large displacement effect, in which deformed configuration is considered in all the equilibrium equations, were included to account for the possible geometric nonlinearity [22]. Figures 4(a) and 4(b) show the analysis models of Pile S-7 and Pile N-7 in Figure 2 in which the lateral spreading modelled as flow displacement and flow pressure, respectively, with the dimensions based on [23]. Details of the models are given as follows.

4.2.1. Modelling of Pile-Soil Interaction. The Winkler foundation model is utilized for the simulation of pile-soil interaction, that is, the pile is modelled by frame elements, and the soil reactions are modelled by spring elements deployed along the pile. However, for the model in Figure 4(b), no soil springs were generated in the flow zone (including the crust and the liquefied layer) for its not providing soil reaction when modelled as flow pressure. Elastic-plastic *p-y* curves for the soil springs are used to represent the nonlinearity of supporting soil. A rigid body constraint was specified to both pile caps to approximate the connection provided by the pile cap as well as the grade beam. To account for the possible flexural failure of piles, the distributed plastic hinge method [24] is adopted. Multiple plastic hinges are inserted along the expected plastic zone of a structural member, because the location of maximum moment along a laterally loaded pile may vary as the nonlinearity of surrounding soil develops. The locations of hinges herein are from the pile head to a depth of 13 m (that is, 1 m below the interface of sand and sandy silt layers), as the green solid circles are shown in Figure 4, and thus, the interface of liquefied and lower nonliquefied layers (at the depth of 9 m) is also covered. Thus, the nonlinear behavior of the pile-soil system can be approximated at an acceptable analysis cost, and the performance of the pile can be assessed according to the damage state judged by the development of plastic hinges.

4.2.2. p-y Curves. In this study, the suggestions of Railway Technical Research Institute, Japan (RTRI) [25] for determining the subgrade reaction coefficient (k_h) for short-term loading as well as the upper bound of the soil reaction to the pile (p_e) were adopted to obtain the *p-y* curves for defining soil springs:

$$k_h = \frac{7200(\mathrm{SPT} - \mathrm{N})}{\gamma_{gE}} D^{-3/4}, \tag{5}$$

$$p_e(z) = 3.0(\overline{\gamma_e} z)\tan^2\left(45^\circ + \frac{\phi}{2}\right), \tag{6}$$

where D denotes the pile diameter; γ_{gE} is the coefficient for subsurface investigation, and a value of 1.3 was used; z is the concerned depth from the ground surface; and $\overline{\gamma_e}$ and ϕ are the average unit weight and the representative friction angle of soil at the depth z.

Because only SPT-N values were available in [16], ϕ was estimated using the following equation (4):

$$\phi = 4.8 \ln N_1 + 21, \tag{7}$$

where N_1 is the corrected SPT-N to an effective overburden stress of 100 kPa.

Equations (5) and (6) give a bilinear elastic-plastic *p-y* relationship as shown in Figure 5, which needs only two parameters to define and is easy to use in engineering practice. Regarding the model in Figure 4(a) (lateral spreading as flow displacement), both k_h and p_e in the liquefied layer were reduced by multiplying D_E listed in Table 2 to consider the soil degradation due to liquefaction, and it is noted that k_h and p_e were reduced to zero at depths of 3~4 m.

4.2.3. Cross-Section and Plastic Hinge Properties of the Piles. The building for case study used Classification A PC piles with a length of 20 m, an outer diameter of 400 mm, and a wall thickness of 65 mm, and their design compressive axial load was 40 tons [16]. The Young modulus $E = 34.3$ GPa and the moment of inertia $I = 0.001025\,\mathrm{m}^4$ of the pile cross-section were specified based on [23]. The properties of plastic hinges on piles were defined moment-curvature (M-ϕ) curves as shown in Figure 6, where M_{cr}, M_y, M_u, and M_{res} denote the cracking moment, yielding moment, ultimate moment, and residual moment of the cross-section of the pile. It should be mentioned that the influence of axial load variation on the properties of the pile cross-section, such as the axial load-bending moment (P-M) interaction, was not included since the comparison of the cases with and without axial load from the superstructure in this study which will be presented later emphasized on the P-delta effect. Considering a Classification A PC pile under a design compressive axial load of 40 tons for simplification [16], it was obtained based on JIS A 5373 [26] that $M_{cr} = 83.3$ kN-m and $M_u = 136.8$ kN-m. In practice, M_y is usually regarded as 0.85-0.95 times of M_u [27–29], and $M_y = 0.9M_u$ was adopted. After cracking, section rigidity of the pile (that is, slope of M-ϕ curve, EI) was reduced to 1/5 of its initial value [23], which was widely adopted in engineering practice. After yielding, a curvature ductility ratio ($\mu_\phi = \phi_u/\phi_y$) of 20 was achieved as the M_u was reached, which gave a section rigidity reduced to 1/400 of its initial value. It is noted that $\mu_\phi = 20$ was based on an allowable displacement ductility ratio (μ) of 4 at pile head

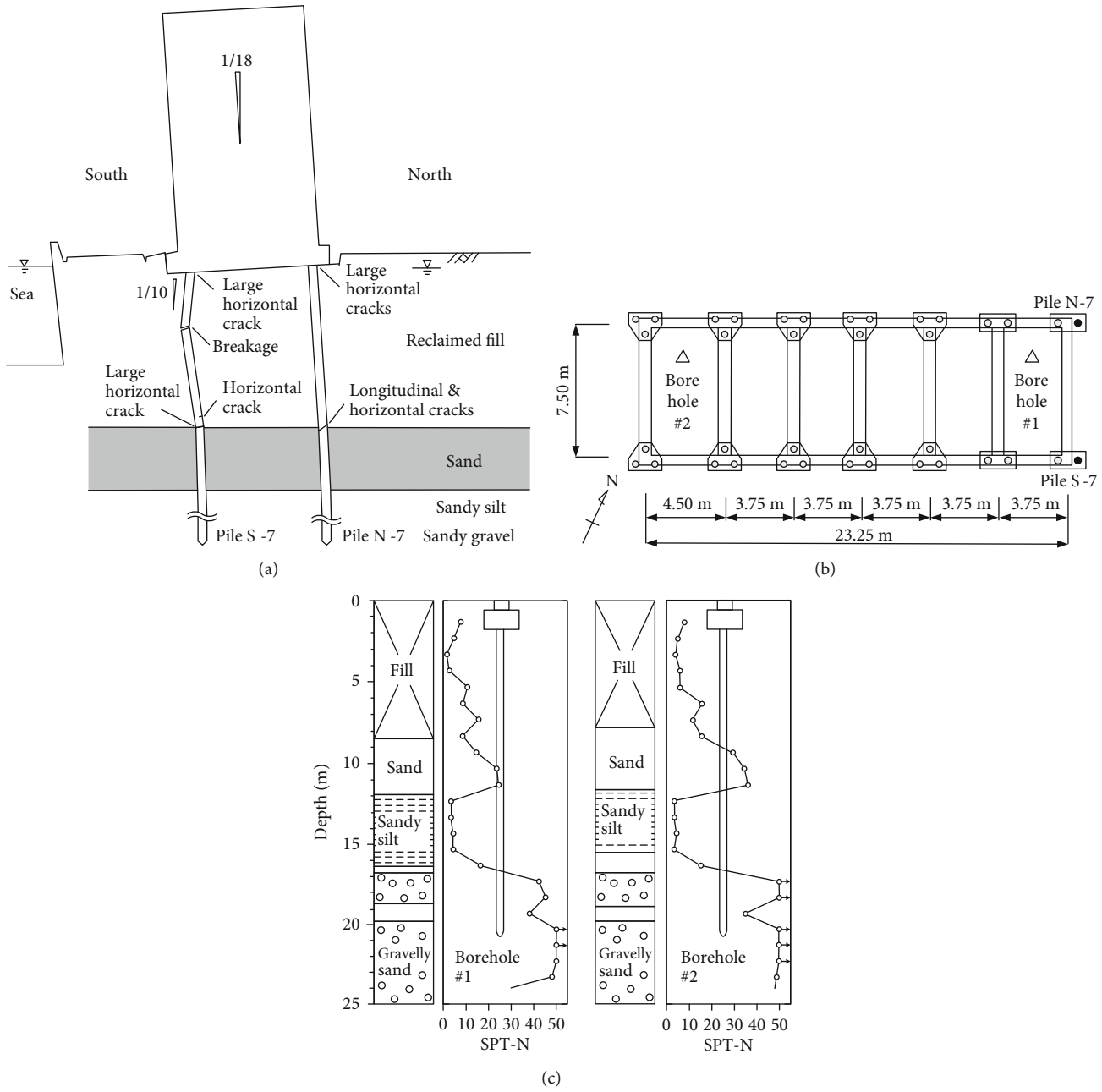

Figure 3: A building near waterfront suffered pile damage during the 1995 Kobe Earthquake. (a) Tilt of the building and damages along piles. (b) Foundation layout. (c) Boring log of the site. (After [16]).

for vertical piles suggested in [4] with the usage of the following equation [30]:

$$\mu_\phi = 1 + \frac{\mu - 1}{3\left(L_p/L\right)\left[1 - 0.5\left(L_p/L\right)\right]}, \tag{8}$$

where L is the pile length; L_p denotes the plastic hinge length and is defined as the spacing between hinges in the distributed plastic hinge method [24].

After reaching M_u, the flexural strength of the pile significantly degraded until a residual moment of $M_{res} = 0.2M_u$ was attained according to FEMA 356 [31] if the pile was regarded as a beam or a column, and this was considered the final state that a complete flexural failure of the pile had occurred.

The mentioned main analysis parameters for the piles are listed in Table 3.

It is noted that the procedure to determine the moment-curvature relationship in this study needs no section analysis and is thus easy for application in engineering practice.

4.2.4. Actions of Lateral Spreading. Concerning the model in Figure 4(a), the flow displacement was assigned using the simplified approximation in [18] mentioned in Section 3.1. Although field observation gave a value up to 1.0 m at Pile

Table 2: Liquefaction potential assessment of the site of case study.

Depth (m)	Soil type	FC (%)	SPT-N	N_1	F_L	D_E
1.00	Fill	10.0	8	17.9	2.15	–
2.00	Fill	10.0	4	6.3	0.82	0.2
3.00	Fill	10.0	1	1.4	0.53	0
4.00	Fill	10.0	2	2.6	0.53	0
5.00	Fill	10.0	10	11.9	0.82	0.2
6.00	Fill	10.0	9	10.1	0.71	0.1
7.00	Fill	10.0	15	15.8	1.14	–
8.00	Fill	10.0	8	8.0	0.61	0.1
9.00	Sand	10.0	14	13.3	0.86	0.2
10.00	Sand	10.0	23	21.0	2.51	–
11.00	Sand	10.0	24	21.0	2.54	–
12.00	Sandy silt	60.0	3	2.6	N.L.	–
13.00	Sandy silt	60.0	3	2.5	N.L.	–
14.00	Sandy silt	60.0	4	3.3	N.L.	–
15.00	Sandy silt	60.0	4	3.2	N.L.	–
16.00	Sandy silt	60.0	16	12.4	N.L.	–
17.00	Gravelly sand	0.0	42	31.7	6.29	–
18.00	Gravelly sand	0.0	46	33.8	9.47	–
19.00	Sand	0.0	38	27.2	2.76	–
20.00	Gravelly sand	0.0	50	34.9	12.0	–

S-7 and around 0.8 m at Pile N-7 [16], these were not free-field displacements but influenced by soil-structure interaction. Therefore, Equation (1) was used to estimate the free-field surface displacement at the piles locations, in which $D_0 = 1.6$ m was specified according to [16], and $L_{ls} = 50D_0 = 80$ m was adopted. It gave a value of 1.23 m at Pile S-7 and 0.88 m at Pile N-7. Then, Equation (2) was utilized for the ground displacement profile, in which $z_w = 2$ m and $H_L = 7$ m were specified based on the liquefaction potential assessment in Section 4.1.

As for the model in Figure 4(b), flow pressure was assigned using Equations (3) and (4), in which $H_{NL} = 2$ m and $H_L = 7$ m were specified. It is noted that, although the flow pressure is dependent on the distance to the waterfront via the coefficient c_s, its values for Pile S-7 and Pile N-7 were the same because the distance were both smaller than 50 m. As the thickness of the nonliquefied crust and liquefied layers was also the same, the obtained pressure profile on both piles was identical.

It is noted that the displacement-control procedure in SAP2000 was adopted when the lateral spreading was modelled as both flow displacement and flow pressure, not only because it has generally better convergence for nonlinear analysis but also because it enables the analysis on structures with a negative stiffness, which is possible herein when the plastic hinge on piles has reached its ultimate moment.

4.3. Analysis Results: Lateral Spreading as Flow Displacement

4.3.1. No Axial Load from Superstructure. Firstly, only the actions of the lateral spreading were considered in terms of flow displacement, and the axial load from the superstructure was neglected. Figure 7 shows the obtained pile deformation, the development of plastic hinges, and the moment distribution along the piles at different structural limit states, of which the yielding state means that the first plastic hinge reached its yielding moment (M_y) so that a significant stiffness reduction of the pile was caused, ultimate state means that the first plastic hinge reached its ultimate moment (M_u) so that the ultimate bending resistance of the pile was attained, and the final state means that the first plastic hinge reached its residual moment (M_{res}) so that a complete flexural failure of the pile was considered having occurred. These mentioned moments are defined in Figure 6.

As 7.0% of the prescribed flow displacement was applied, the yielding state was reached though the pile cap displacement was merely slightly above 0.07 m. Plastic hinges beyond cracking on Pile S-7 showed at the depth of 4-6 m (refer to Table 2, near the border between soil springs with $D_E = 0$ and $D_E > 0$) as well as near the interface of liquefied and lower nonliquefied layers, where the first yielding hinge appeared (at a depth of 9 m), while those on Pile N-7 were mainly near the pile head. When 66.1% of the prescribed flow displacement was applied, the pile cap displacement was about 0.7 m, and the ultimate state was reached because the first hinge attained its M_u on Pile S-7 at a depth of 9 m, and the majority of the plastic hinges in the liquefied layer on both piles had yielded. As all the prescribed flow displacement was eventually imposed to the piles, the displacement at the pile cap was 1.08 m, conforming to the field observations, and the moment resistance in the plastic hinge on Pile S-7 at a depth of 9 m had descended to M_{res}, indicating that the final state had been reached; meanwhile, the hinge on Pile N-7 at the depth of 9 m had attained its M_u.

Naturally, the locations of plastic hinges can be related to the extrema of the moment distribution curves shown in Figure 7; moreover, a double-curvature behavior of both piles is noticed by the sign change of the bending moment except for Pile N-7 at the final state because the hinge reaching M_{res} served as a fuse to prevent the downward transmission of the moment. This double curvature is probably due to the restraints from the pile cap and the grade beam at the upper ends of the piles as well as from the soil reaction of the lower nonliquefied layer.

Excluding the plastic hinges at the interface of liquefied and lower nonliquefied layers, the distribution of hinges, though mainly in the liquefied layer, was somewhat different on Pile S-7 and Pile N-7. For the former, plastic hinges with a worse damage state concentrated in the middle of the pile sector in the liquefied layer, while those for the latter were closer to the upper and lower ends. This difference can be attributed to the discrepancy in moment distribution. Anyhow, development of plastic hinges roughly meets the real situation in which piles were more severely damage near the pile head as well as near the border between reclaimed fill and sand (namely, between liquefied and lower nonliquefied layers), as shown in Figure 3(a). However, it is also noted the breakage of Pile S-7 at a depth of 4.5 m was not reproduced in the analysis, even though a considerable pile sector around

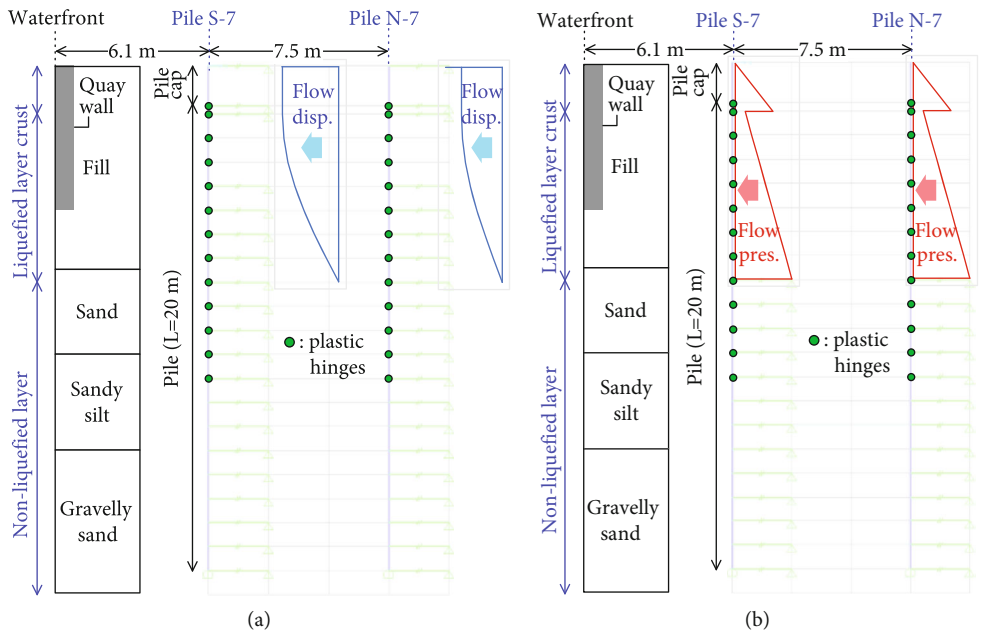

Figure 4: SAP2000 model for case study. (a) Lateral spreading as flow displacement. (b) Lateral spreading as flow pressure.

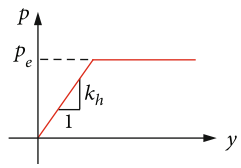

Figure 5: Bilinear elastic-plastic p-y curve.

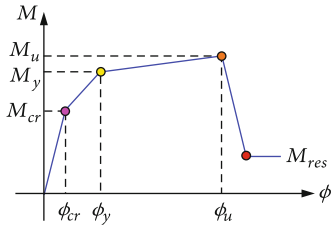

Figure 6: Moment-curvature curve to define plastic hinges on piles (not to scale).

this depth had reached yielding. This will be further discussed in the next section.

4.3.2. With Axial Load from Superstructure. As mentioned in Section 4.2.3, the design compressive axial load of the pile in this case was 40 tons. Therefore, in this case, the 40-ton axial load was further applied as concentrated load before the action of lateral spreading and remained constant during the analysis to investigate its influence on the pile performance. The axial load on each pile would vary in reality as the structure was subjected to different levels of lateral actions due to the restraint of grade beams and pile caps. However, including axial load variation would make the analysis rather complicated because it could be necessary to model the superstructure, and in addition, the P-delta effect could not be conspicuously exhibited. Therefore, a constant compressive axial load was adopted for both simplification and better demonstration. Figure 8 depicts the pile deformation, the development of plastic hinges, and the moment distribution along the piles.

The yielding state was reached as 6.6% of the prescribed flow displacement was applied, and the pile cap displacement as well as the distribution of plastic hinges were similar to the no-axial-load case. The ultimate state was reached when 65.2% of the prescribed flow displacement was applied, and the first hinge attained its M_u on Pile S-7 also at a depth of 9 m, yet meanwhile, the pile cap displacement was nearly 0.8 m, larger than the no-axial-load case. It is also noticed that more plastic hinges on Pile S-7 in the liquefied layer had yielded but less on Pile N-7. The final state had been reached when all the prescribed flow displacement was imposed to the piles because the plastic hinge on Pile S-7 at a depth of 9 m had attained its M_{res}, same as the no-axial-load case, and meantime, the hinge on Pile N-7 at the depth of 9 m had also attained its M_u. However, the displacement at the pile cap was up to 1.22 m, larger than the no-axial-load case.

The discrepancy between the analyses with and without the axial load is probably due to the additional moment from the axial load as the pile head was laterally displaced, or the P-delta effect. This additional moment is responsible for greater displacement of the pile cap, the slightly earlier reaching of the yielding and ultimate states, and the larger yielding zone of Pile S-7 in the liquefied layer. Although the breakage of Pile S-7 at a depth of 4.5 m was still not reproduced, the P-delta effect did cause the more extensive damage of Pile S-7. Further considering the total loss of soil resistance ($D_E = 0$) near this depth due to severe liquefaction that can be regarded as the absence of lateral confinement of the pile,

Table 3: Main analysis parameters for piles.

Cross-section properties				
Length	Outer diameter	Thickness	Young's modulus, E	Moment of inertia, I
20 m	400 mm	65 mm	34.3 GPa	0.001025 m^4
Plastic hinge properties				
Cracking moment, M_{cr}	Yielding moment, M_y	Ultimate moment, M_u	Residual moment, M_{res}	Curvature ductility ratio, μ_ϕ
83.3 kN-m	123.1 kN-m	136.8 kN-m	27.4 kN-m	20

the buckling instability of Pile S-7 might be induced. Unfortunately, it could not be represented by the displacement-based approach despite the P-delta effect had been included in the analysis.

It should be mentioned that the two piles were possibly subjected to different axial loads in reality, which might influence their damage patterns. Although the analysis model can account for this possibility, yet for this case, the design axial load was adopted because the purpose was to exhibit the effect of the axial load. Consequently, discrepancy between the damage patterns from the analysis and of the reality could be thus caused.

4.4. Analysis Results: Lateral Spreading as Flow Pressure

4.4.1. No Axial Load from Superstructure. Similarly, the axial load from the superstructure was firstly neglected, and only the actions of the lateral spreading were considered in terms of flow pressure. The pile deformation, the development of plastic hinges, and the moment distribution along the piles at different structural limit states are given in Figure 9.

The yielding state was reached with the appearance of yielding hinges on both Pile S-7 and Pile N-7 at a depth of 9 m, the interface of liquefied and lower nonliquefied layers, until 61% of the prescribed flow pressure was applied, yet meantime, the pile cap displacement was merely 0.087 m. In addition, development of plastic hinges on both piles were the same, beyond cracking near the pile head as well as near the depth of 9 m, which can be related the almost identical moment distribution on both piles which showed a double curvature with the moment extrema at the pile head and at a depth of 9 m. The identical moment distribution was due to the same pressure profile acting on both piles as well as the symmetric structure. As 73% of the prescribed flow pressure was imposed, the pile cap displacement was about 1.17 m, and on both piles, the hinges at a depth of 9 m firstly attained their M_u, showing that the ultimate state was reached; meanwhile, both piles yielded near the pile head. After this, no additional flow pressure could be applied, probably because the moment-curvature relationship of the hinges having reached their M_u showed a negative slope, as shown in Figure 6; that is, the moment resistance was descending. Further examining the base shear of the model versus the pile cap displacement, as shown in Figure 10, a negative slope of the curve that represented the negative stiffness of the foundation system exhibited after its ultimate state, indicating that the system was unstable. Thus, the final state defined as one of the hinges reached its M_{res} was not available.

In this case, damage near the pile head and the interface between reclaimed fill and sand can be approximated, but the breakage of Pile S-7 at a depth of 4.5 m was still not reproduced. In addition, as mentioned, the damage pattern of Pile S-7 and Pile N-7 were identical in the analysis, yet this is not conformable to the real situation that some difference existed.

4.4.2. With Axial Load from Superstructure. When the design compressive axial load of 40 tons was included, the yielding state was reached as 52% of the prescribed flow pressure was applied, and the yielding hinges also appeared on both Pile S-7 and Pile N-7 at a depth of 9 m, as shown in Figure 11. Although at this moment the pile cap displacement was only 0.125 m, no additional flow pressure could be applied afterwards. The base shear of the model versus the pile cap displacement of this case, as shown in Figure 10, exhibited greater discrepancy from the no-axial-load case as the pile cap displacement increased, and consequently, a negative stiffness of the foundation system was shown after its yielding state; that is, the foundation system was unstable, and thus, the ultimate and final states were both not available. Since the moment-curvature relationship of the plastic hinges in Figure 6 exhibits a hardening tendency after yielding, this negative stiffness can be attributed to the P-delta effect shown with the inclusion of the compressive axial load, which is often considered equivalent to reduction of flexural rigidity of a structural member, and can be regarded as the occurrence of buckling. P-delta effect was also responsible for the less applied flow pressure and larger pile cap displacement at yielding than in the no-axial-load case.

The damage pattern of the piles shown in Figure 11 is similar to in Figure 9(a), the no-axial-load case. Despite the breakage of Pile S-7 at a depth of 4.5 m was also not directly reproduced in the analysis, the negative stiffness of the foundation system owing to the P-delta effect occurred before its ultimate state implied that the buckling instability might control the failure of the piles, which was considered possible for slender piles, especially for those embedded in liquefied ground. That is, the complete damage of Pile S-7 at a depth of 4.5 m was probably related to the buckling of the pile sector in the liquefied layer.

4.5. Comparison and Discussions. Some differences are noticed in the results of the displacement-based and force-

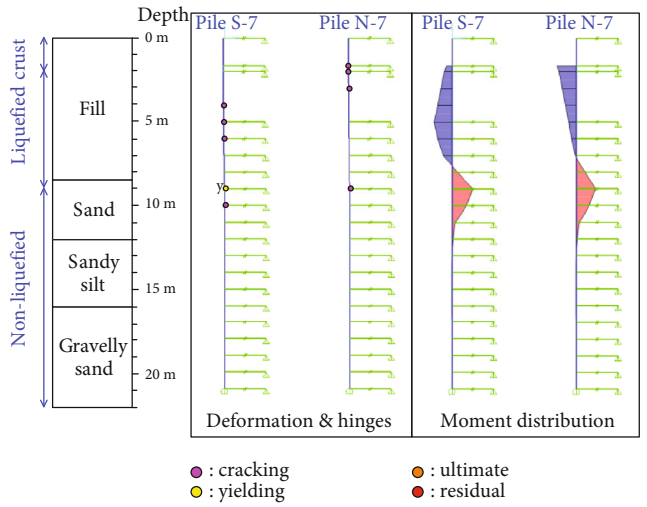

(a)

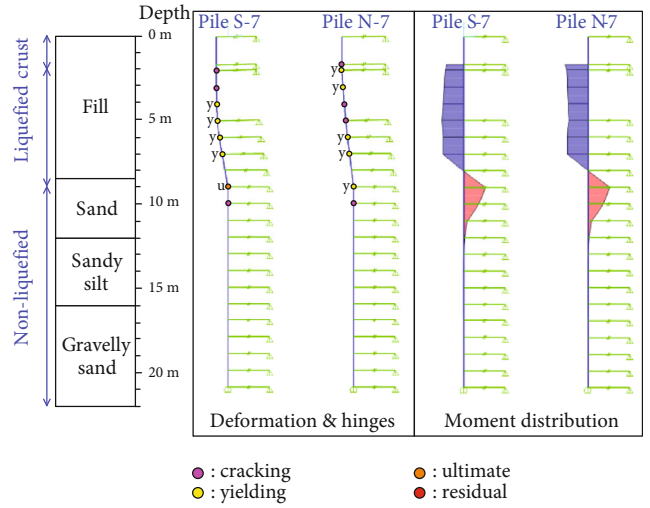

(b)

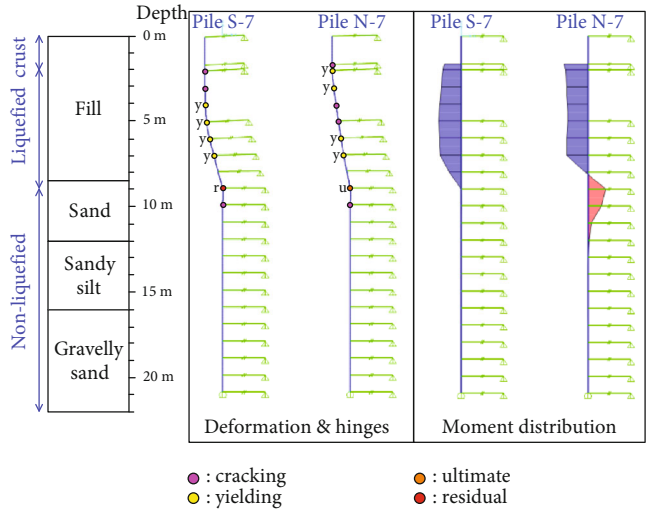

(c)

Figure 7: Deformation, plastic hinges, and moment distribution along the piles (lateral spreading as flow displacement, no axial load). (a) Yielding state. (b) Ultimate state. (c) Final state.

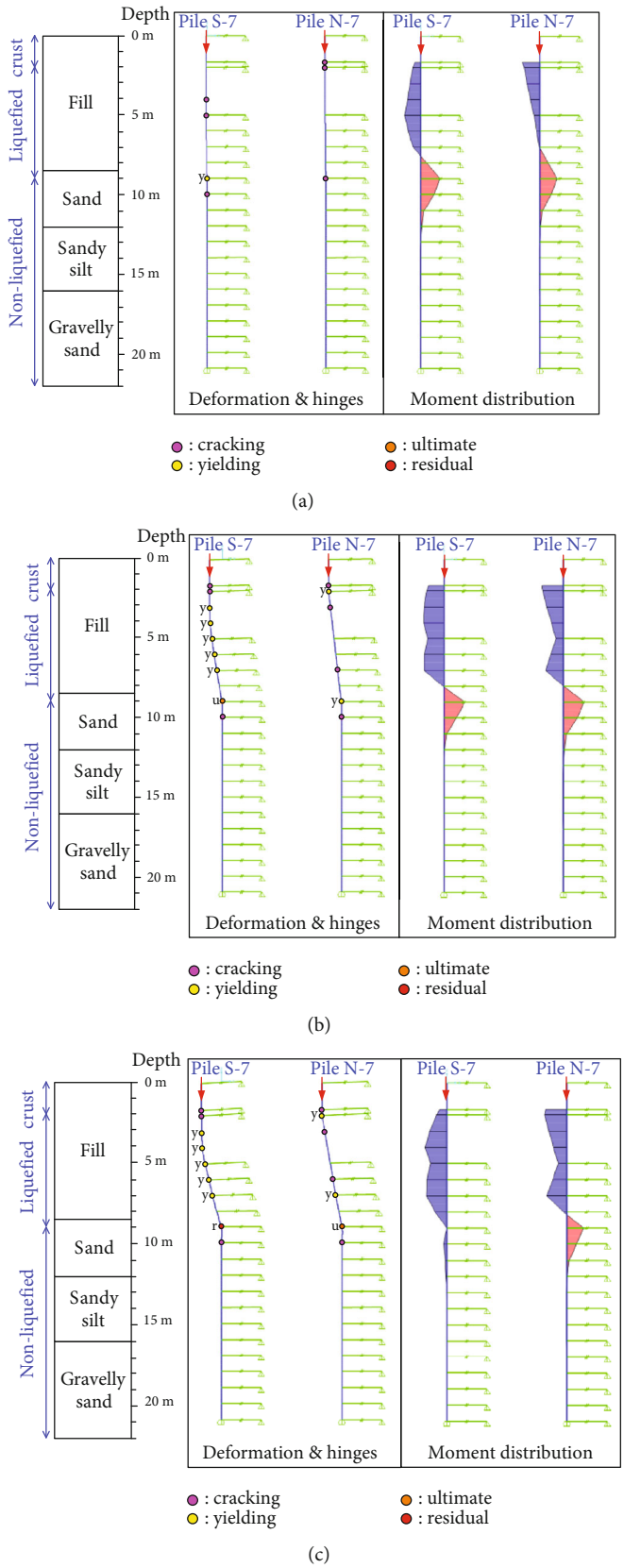

Figure 8: Deformation, plastic hinges, and moment distribution along the piles (lateral spreading as flow displacement, with axial load). (a) Yielding state. (b) Ultimate state. (c) Final state.

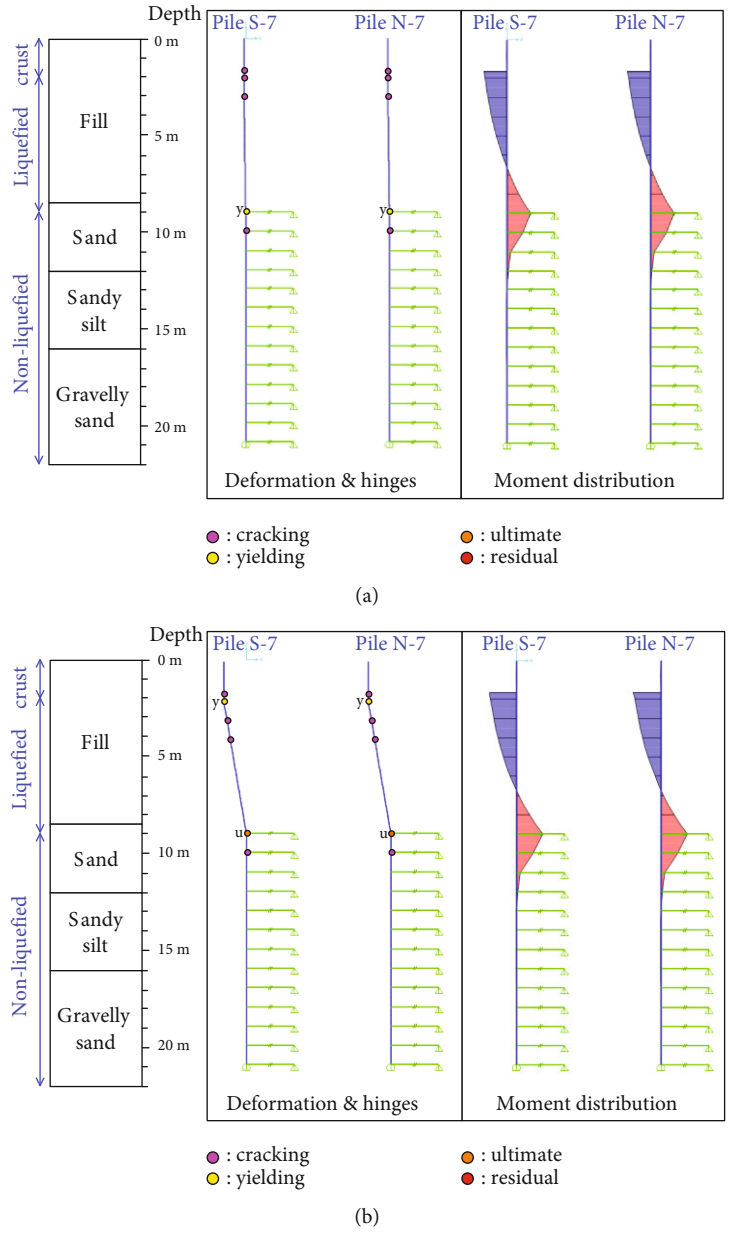

Figure 9: Deformation, plastic hinges, and moment distribution along the piles (lateral spreading as flow pressure, no axial load). (a) Yielding state. (b) Ultimate state. (Final state not available).

based approaches. The most obvious one is that the prescribed actions of lateral spreading could not be entirely applied in the latter, because the foundation system had a negative stiffness and was thus unstable after a certain damage state, while using the former enabled the complete imposition of the action. Additionally, the pile cap displacement obtained using the force-based approach was more conservative (larger) either in the yielding state or in the ultimate state, while that obtained using displacement-based approach when all the prescribed flow displacement had been applied was close to field observations.

The flow pressure profile proposed in [4] is basically corresponding to a limit state in which the passive earth pressure is developed in the nonliquefied crust layer. However, based on the comparison of the simplified analysis [2] and the centrifuge test results [5], modelling lateral spreading as flow pressure could be overpredicted the bending moments in the pile if the ground movements were not large enough to mobilize the presumed limit pressures. In other words, the assigned flow pressure, especially that in the nonliquefied crust layer, could be overestimated and thus more conservative compared to the real situation.

Another discrepancy is the moment distribution of the piles, which was very similar in both piles when the force-based approach was used, thus leading to identical damage pattern. On the other hand, using the displacement-based

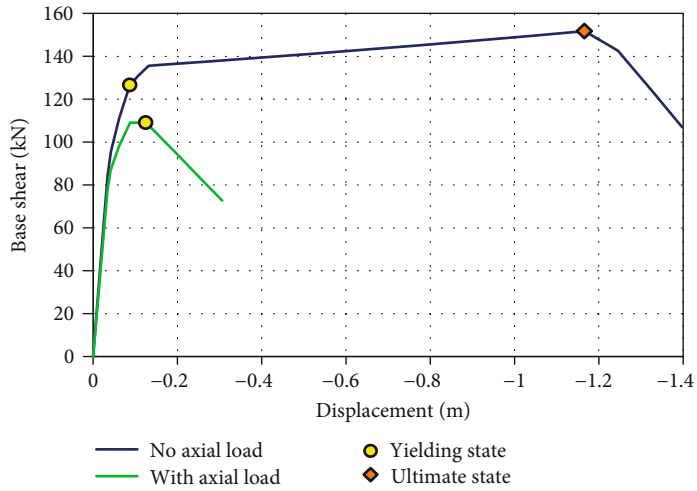

Figure 10: Base shear versus pile cap displacement (lateral spreading as flow pressure).

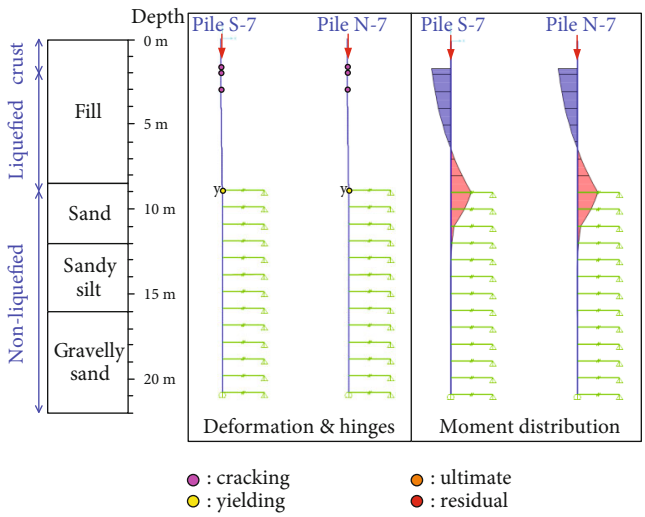

Figure 11: Deformation, plastic hinges, and moment distribution along the piles (lateral spreading as flow pressure, with axial load) at yielding state (ultimate and final states not available).

approach gave different moment distribution in the piles, and consequently, Pile S-7 was more severely damaged, which was conformable to the real situation. The reason could be that the adopted method to estimate flow pressure [4] in the force-based approach only roughly takes the distance from the waterfront into consideration via the factor c_s, and in this case, the same c_s was specified for both piles so that identical flow pressure was assigned; while in the displacement-based approach, different flow displacement profile was estimated according to [18] for each pile, because different ground surface displacement was specified considering its distance from the waterfront.

To further clarify the action of lateral spreading in both approaches, though the displacement-based one is basically forced displacement analysis and thus the lateral spreading pressure cannot be directly obtained, the lateral reaction of each soil spring as all the prescribed displacement profile had been imposed was used to calculate the apparent-pressure diagram along both piles, which was from the idea from the braced cut analysis. It was then compared to the flow pressure profile used in the force-based approach, as shown in Figure 12, where positive values denote pressure from the north (landside) whereas negative values denote pressure from the south (seaside) (refer to Figure 3(a)). Large discrepancy was noticed, because the apparent pressure varied intensely with respect to the depth and did not drop to zero below the liquefied layers. However, it should be emphasized that this apparent pressure distribution were in fact the consequence of the pile-soil interaction and could be significantly influenced by the structural characteristics of the piles, such as the rigid body constraint specified to both pile caps which made this interaction more complicated. On the other hand, the flow pressure profile was based on limit state of soil [4] and was irrelevant to the structure. It could be roughly regarded as the lateral spreading pressure acting on a rigid structure if the ground movements were large enough for limit pressure mobilization, yet this also means the pile-soil interaction was excluded.

To conclude, the flow displacement seems to better approximate the actions of liquefaction-induced lateral spreading in this case. Nevertheless, the displacement-based method, which basically performs the analysis by imposing given displacement profile as boundary conditions without actually applying lateral spreading pressure, cannot explicitly exhibit the instability due to either the strength descending of structure members or the geometric nonlinearity, because no base shear can be directly output by the SAP2000 software during the analysis. By contrast, the instability can be represented by the force-based method in terms of the negative stiffness of the foundation system, namely, the negative slope of the curve showing base shear versus pile cap displacement. If the flow pressure can be adjusted to consider the level of limit pressure mobilization and the distance from the waterfront more specifically, as well as to include the influences of the

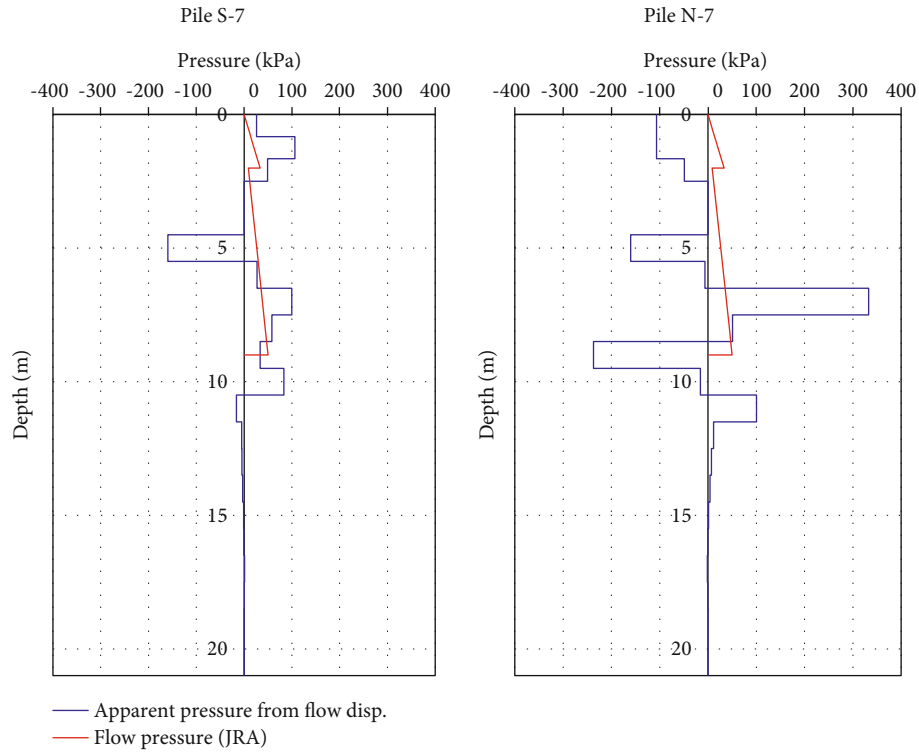

Figure 12: Comparison of apparent-pressure diagram from the displacement-based approach and the flow pressure used in the force-based approach.

soil-structure interaction on the actions of lateral spreading, the force-based method can be expected to capture main damage patterns of piles subjected to lateral spreading and can thus reasonably assess their performance.

5. Applicability and Limitations

The proposed analysis model basically utilizing the concept of the Winkler foundation, which only needs beam-column (frame) and spring elements. The soil nonlinearity is represented by nonlinear *p-y* curves, and the possible flexural failure (or even shear failure) of piles is simulated by plastic hinges. Therefore, the model can be established by any of the recognized structural analysis codes as long as it allows of defining nonlinear force-displacement relationship of the spring elements and provides plastic hinges, which makes this model quite applicable in engineering practice.

However, an apparent limitation of the model noticed in the analysis results is that it failed to specifically reproduce the buckling-induced damage of the pile. Although the model was able to account for P-delta effect when axial load on the pile was included, it could only simulate the consequently caused additional moment when the laterally spreading ground was modelled as flow displacement but the instability due to the nature of displacement-based approach. To be more specific, the approach comprised forced displacement analysis which was made with given displacement boundary conditions, and thus, an equilibrium solution could always be obtained at a prescribed flow displacement profile as long as the strength of the pile-soil system was still enough to resist the action of the axial load. Therefore, it cannot highlight the possible structural instability under the combination of lateral spreading and axial load. On the other hand, the force-based approach could exhibit the instability in terms of negative stiffness of the pile-soil system after its yielding but before ultimate states when axial load was considered. However, it also means no additional flow pressure could be applied at this moment, because the analysis scheme needed to achieve an equilibrium, and thus, the sequential structural failure was not reproduced. To this end, an explicit scheme allowing for the simulation of failure or even collapse process of structures may be necessary.

Nevertheless, revealing the possibility of geometrical instability, which the proposed model is capable of, is still beneficial in engineering practice. Thus, this model can be considered competent for the need of performance assessment. For instance, if negative stiffness of the pile-soil system, either caused by the strength degradation of the pile-soil system or by geometric nonlinearity, is exhibited using the force-based model, the performance of the piles can be regarded as nearly collapse.

Another limitation for the force-based approach, though it is preferable considering the buckling of piles, is the modelling of flow pressure. According to the results of case study, it gave larger displacement and failed to approximate the damage pattern, and the reason could be that the flow pressure profile proposed by JRA [4] was not sufficiently adequate. This is an important issue to be investigated in the future.

6. Conclusions

In this study, the response of piles subjected to lateral spreading of liquefied ground was evaluated using nonlinear pseudo-static analysis, and a pile damage case during the 1995 Kobe Earthquake was adopted for case study. The actions of laterally spreading ground were modelled as both flow displacement and flow pressure, and the results were compared and discussed. Several conclusions can be drawn as follows:

(1) By the usage of the Winkler foundation with soil springs represented by elastic-plastic *p-y* curves to account for the pile-soil interaction, and the distributed plastic hinges on the pile to simulate its flexural failure, as well as the inclusion of P-delta effect, the nonlinear behavior, and the damage pattern of laterally loaded piles can be reasonably approximated at an acceptable cost for engineering practice purpose. Thus, the performance of piles can be assessed according to the status of the plastic hinges and the stability of the analysis model

(2) The displacement-based approach with the flow displacement estimated following Tokimatsu and Asaka [18] gave a damage pattern in which considerable damages were caused to both piles near the pile head and the interface between the liquefied and lower nonliquefied layers, and the latter was the most severe, while Pile S-7 was also severely damaged in the middle of its sector in the liquefied layers. This is roughly conformable to the reality except the pile breakage at a depth of 4.5 m was not successfully reproduced. In addition, the obtained pile cap displacement was also close to the field observations. By contrast, the force-based approach with the flow pressure profile proposed by JRA [4] gave somewhat different damage pattern and more conservative pile cap displacement compared to the displace-based approach

(3) Including the compressive axial load of piles caused the same damage state to be reached at a lower magnitude of applied actions and larger corresponding pile cap displacement, that is, it intensified the flexural damage of laterally loaded pile. This can be owing to the additional moment from the P-delta effect. Hence, the axial load should be considered in evaluating the lateral resistance of piles

(4) Despite of the somewhat different results compared to the real case, the force-based method can account for the structural instability of the pile due to either strength descending of plastic hinges or the geometric nonlinearity in terms of the negative stiffness of the foundation system, which helps to capture the dominant failure mode of the pile in assessing its performance. Accordingly, buckling failure was possible for the pile in the investigated case when the compressive axial load was included, because the global instability occurred before the ultimate moment of any of the plastic hinges was reached. By contrast, the displacement-based method cannot highlight this instability, because an equilibrium solution can always be obtained at the prescribed flow displacement as long as the structure is still adequate to resist the axial load

Data Availability

The data used to support the findings of this study are included within this article.

Conflicts of Interest

The authors declare that they have no conflict of interest regarding the publication of this article.

Acknowledgments

The research and publication of this article was funded by the in-house project: Study on the seismic performance of geotechnical structures of National Center for Research on Earthquake Engineering, National Applied Research Laboratories, Taiwan.

References

[1] S. Bhattacharya and K. Tokimatsu, "Collapse of Showa Bridge revisited," *International Journal of Geoengineering Case Histories*, vol. 3, no. 1, pp. 24–35, 2013.

[2] S. J. Brandenberg, R. W. Boulanger, B. L. Kutter, and D. Chang, "Static pushover analyses of pile groups in liquefied and laterally spreading ground in centrifuge tests," *Journal of Geotechnical and Geoenvironmental Engineering*, vol. 133, no. 9, pp. 1055–1066, 2007.

[3] S. A. Ashford, R. W. Boulanger, and S. J. Brandenberg, *Recommended Design Practice for Pile Foundations in Laterally Spreading Ground*, PEER, Berkeley, CA, 2011.

[4] Japan Road Association (JRA), *Specifications for Highway Bridges*, Part V – Seismic Design, Japan Road Association, Tokyo, Japan, 2012, (in Japanese).

[5] A. F. Rauch, *EPOLLS: An Empirical Method for Predicting Surface Displacements Due to Liquefaction– Induced Lateral Spreading in Earthquakes, Ph.D. dissertation*, Virginia Polytechnic Institute and State University, VA, 1997.

[6] T. L. Youd, "Liquefaction-induced lateral ground displacement," in *Proceedings of 3rd International Conference on Recent Advances in Geotechnical Earthquake Engineering and Soil Dynamics*, vol. 2, pp. 911–925, St. Louis, MS, USA, April 1995.

[7] K. Tokimatsu, H. Mizuno, and M. Kakurai, "Building damage associated with geotechnical problems," *Soils and Foundations*, vol. 36, pp. 219–234, 1996.

[8] M. Cubrinovski and K. Ishihara, "Simplified method for analysis of piles undergoing lateral spreading in liquefied soils," *Soils and Foundations*, vol. 44, no. 5, pp. 119–133, 2004.

[9] S. J. Brandenberg, R. W. Boulanger, B. L. Kutter, and D. Chang, "Behavior of pile foundations in laterally spreading ground during centrifuge tests," *Journal of Geotechnical and Geoenviromental Engineering*, vol. 131, no. 11, pp. 1378–1391, 2005.

[10] S. M. Haeri, A. Kavand, I. Rahmani, and H. Torabi, "Response of a group of piles to liquefaction–induced lateral spreading by large scale shake table testing," *Soil Dynamics and Earthquake Engineering*, vol. 38, pp. 25–45, 2012.

[11] R. Motamed, I. Towhata, T. Honda, K. Tabata, and A. Abe, "Pile group response to liquefaction–induced lateral spreading: E–Defense large shake table test," *Soil Dynamics and Earthquake Engineering*, vol. 51, pp. 36–46, 2013.

[12] R. Dobry, T. Abdoun, T. D. O'Rourke, and S. H. Goh, "Single piles in lateral spreads: field bending moment evaluation," *Journal of Geotechnical and Geoenvironmental Engineering*, vol. 129, no. 10, pp. 879–889, 2003.

[13] National Institute of Standards and Technology (NIST), *The January 17, 1995 Hyogoken–Nanbu (Kobe) Earthquake – Performance of Structures, Lifelines, and Fire Protection Systems, NIST Special Publication 901, Building and Fire Research Laboratory*, National Institute of Standards and Technology, Gaithersburg, MD, 1996.

[14] PIANC (World Association for Waterborne Transport Infrastructure), *Seismic Design Guidelines for Port Structures*, A.A. Balkema Publishers, Lisse, Netherlands, 2001.

[15] K. Ishihara and M. Cubrinovski, "Case studies of pile foundations undergoing lateral spreading in liquefied deposits," in *5th International Conference on Case Histories in Geotechnical Engineering*, New York, NY, USA, April 2004.

[16] K. Tokimatsu, H. Oh-oka, K. Satake, Y. Shamoto, and Y. Asaka, "Failure and deformation modes of piles due to liquefaction-induced lateral spreading in 1995 Hyogoken–Nambu earthquake," *Journal of Structural and Construction Engineering, AIJ*, vol. 62, no. 495, pp. 95–100, 1997, (in Japanese).

[17] M. Cubrinovski, J. D. Bray, C. de la Torre et al., "Liquefaction effects and associated damages observed at the Wellington Centreport from the 2016 Kaikoura earthquake," *Bulletin of the New Zealand Society for Earthquake Engineering*, vol. 50, no. 2, pp. 152–173, 2017.

[18] K. Tokimatsu and Y. Asaka, "Effects of liquefaction–induced ground displacements on pile performance in the 1995 Hyogoken–Nambu earthquake," *Soil and Foundations*, vol. 38, pp. 163–177, 1998.

[19] T. Iwasaki, T. Arakawa, K. Tokida, and S. Yasuda, "A practical method for assessing soil liquefaction potential based on case studies at various sites in Japan," in *Proceedings of 2nd International Conference on Microzonation for Safer Construction - Research and Application*, vol. 2, pp. 885–896, San Francisco, CA, USA, November-December 1978.

[20] AIJ (Architectural Institute of Japan), *Recommendations for Design of Building Foundations*, Architectural Institute of Japan, Tokyo, Japan, 2001, (in Japanese).

[21] J. H. Huang and C. H. Chen, "Evolution of design guidelines on soil liquefaction assessment," *Sino-Geotechnics*, vol. 70, pp. 23–44, 1998, (in Chinese).

[22] CSI (Computers & Structures, Inc), *CSI Analysis Reference Manual for SAP2000 Ver. 20*, Walnut Creek, CA, 2017.

[23] R. Uzuoka, N. Sento, A. Yashima, and F. Zhang, "3–dimensional effective stress analysis of a damaged group–pile foundation adjacent to a quay wall," *Journal of JAEE*, vol. 2, no. 2, pp. 1–14, 2002, (in Japanese).

[24] J. S. Chiou, H. H. Yang, and C. H. Chen, "Use of plastic hinge model in nonlinear pushover analysis of a pile," *Journal of Geotechnical and Geoenvironmental Engineering*, vol. 135, no. 9, pp. 1341–1346, 2009.

[25] RTRI (Railway Technical Research Institute), *Design Standards for Railway Structures and Commentary (Substructures)*, Railway Technical Research Institute, Tokyo, Japan, 2012, (in Japanese).

[26] Japanese Standards Association (JSA), *Japanese Industrial Standard JIS A 5373: 2004 – Precast Prestressed Concrete Products*, Japanese Standards Association, Tokyo, Japan, 2004.

[27] H. G. Kwak and S. P. Kim, "Nonlinear analysis of RC beams based on moment–curvature relation," *Computers and Structures*, vol. 80, no. 7–8, pp. 615–628, 2002.

[28] K. Watanabe, Y. Umemura, M. Teshigawara, M. Iiba, and M. Tamura, "A study on seismic response evaluation by monolithic analysis of building and its foundation," in *13th World Conference on Earthquake Engineering (13WCEE)*, Vancouver, B.C., Canada, August 2004.

[29] Z. Guo, *Strength and Constitutive Relationship for Concrete – Mechanism and Application*, China Industrial and Building Press, Beijing, China, 2004, (in Chinese).

[30] T. Paulay and M. J. N. Priestley, *Seismic Design of Reinforced Concrete and Masonry Buildings*, John Wiley & Sons, New York, 1992.

[31] American Society of Civil Engineers (ASCE), *Prestandard and commentary for the seismic rehabilitation of buildings*, Report FEMA 356 Federal Emergency Management Agency, Washington, D.C., USA, 2000.